Journal of Solid State Chemistry 182 (2009) 2985–2990

Contents lists available at ScienceDirect

Journal of Solid State Chemistry

journal homepage: www.elsevier.com/locate/jssc

Hydrothermal synthesis of yttria stabilized ZrO_2 nanoparticles in subcritical and supercritical water using a flow reaction system

Hiromichi Hayashi *, Akiko Ueda, Atsuko Suino, Kyoko Hiro, Yukiya Hakuta

Research Center for Compact Chemical Process, National Institute of Advanced Industrial Science and Technology (AIST), Nigatake 4-2-1, Miyagino-ku, Sendai 983-8551, Japan

ARTICLE INFO

Article history:
Received 1 July 2009
Received in revised form
7 August 2009
Accepted 11 August 2009
Available online 15 August 2009

Keywords:
Yttria stabilized zirconia
Hydrothermal synthesis
Supercritical water
Nanoparticle
Particle size

ABSTRACT

Yttria stabilized zirconia nanoparticles have been prepared by hydrothermal flow reaction system under subcritical and supercritical conditions. $ZrO(NO_3)_2$/$Y(NO_3)_3$ mixed solutions were used as starting materials. Reaction temperature was 300–400 °C. Reaction time was adjusted to 0.17–0.35 s. Based on the residual Zr and Y concentrations, the complete conversion of zirconium was achieved irrespective of pH and hydrothermal temperature, whereas the conversion of yttrium increased with an increase in pH and hydrothermal temperature. Stoichiometric solid solution was achieved at pH > 8. XRD results revealed that tetragonal zirconia can be formed regardless of yttrium content, where the tetragonality was confirmed by Raman spectroscopy. The average particle size estimated from BET surface area was around 4–6 nm. Dynamic light scattering particle size increased with the solution pH owing to the aggregation of primary particles. TG-DTA analyses revealed that weight losses for adsorbed water and hydroxyl groups decreased with hydrothermal temperature.

1. Introduction

Zirconia and yttria stabilized zirconia ceramics are used widely in the field of industrial materials such as structural ceramics [1], solid catalysts [2–4], oxygen sensor [5,6], electric materials or oxygen electrolyte for solid oxide fuel cells [7,8], etc. Zirconia particles are prepared commercially by precipitation or hydrolysis methods [9–11]. Several methods have been developed for producing zirconia nanoparticles such as pyrolysis [12–15], sol–gel [16,17], citrate complex [18–21], microwave [22], and hydrothermal synthesis [23–31] methods. Recently, solvothermal [32] and supercritical water processes [33] have been proved to be advantageous in nanoparticle formation. Key features of the supercritical hydrothermal synthesis method have been identified. Ultrafine particles are produced; morphology and particle sizes can be controlled by the operation conditions. Additionally, the flow-type reaction system provides couple of advantages to the supercritical hydrothermal synthesis. First, a sudden change in the dielectric constant of the reaction medium results in the high-density homogeneous nucleation. Second, a very short reaction time can suppress the crystal growth. Thus the rapid and continuous synthesis method affords relatively narrow particle size distribution of metal oxides nanoparticles.

Zirconia nanocrystals have been prepared by hydrothermal reaction of zirconyl nitrate or zirconyl acetate solutions in supercritical water [34]. The reaction rate of hydrolysis of zirconyl nitrate is extremely high and almost complete conversion was attained even in acidic solutions at 400 °C. According to XRD analyses, amorphous hydrous zirconia formed regardless of the starting metal salt. However, amorphous zirconia transformed through tetragonal phase to stable monoclinic phase. The size of the primary particles was around 6 nm and did not change during phase transformation. These results suggest that the crystallization and phase transformation of zirconia nanocrystals were advanced by a solid state process rather than dissolving-crystallization process.

Zirconia exhibits three primary polymorphs: monoclinic, tetragonal and cubic, in which tetragonal phase has been applicable to a number of technologies. Tetragonal zirconia is thermodynamically metastable at ambient conditions, thus doping of ceria and yttria is utilized to stabilize the tetragonal phase. The zirconia and ceria-zirconia solid solution particles have been already produced by hydrothermal flow reaction system. $Ce_{1-x}Zr_xO_2$ solid solutions were produced continuously by hydrolysis of mixtures of cerium ammonium nitrate and zirconium acetate at 300 °C and 25 MPa using a flow reactor. Rapid hydrothermal coprecipitation can be achieved for the $Ce_{1-x}Zr_xO_2$ ($x = 0$–1) nano-particulate and the tetragonal phase was obtained in the range $0.8 < x < 0.9$ [35,36]. However, hydrothermal synthesis of yttria stabilized zirconia nanoparticles using flow reaction system in wide pH range has not been reported, whereas $Ce_xZr_yY_zO_{2-\delta}$

* Corresponding author. Fax: +81 22 237 5215.
E-mail address: h-hayashi@aist.go.jp (H. Hayashi).

0022-4596/$ - see front matter © 2009 Elsevier Inc. All rights reserved.
doi:10.1016/j.jssc.2009.08.013

nanocrystals have been synthesized by a novel high-throughput continuous hydrothermal flow reaction system in basic solutions [37]. Compared with the ceria, yttria cannot readily substitute the zirconium sites since the solubility of yttria might be higer than that of ceria.

In the present study, our objective was to synthesize yttria stabilized zirconia (YSZ) single nanoparticles in one step. Thus, formation and crystallization of YSZ nanocrystals have been investigated by a flow hydrothermal reaction system under sub- and supercritical water conditions. Hydrothermal reaction for the formation of YSZ was conducted by controlling the parameters of solution pH, yttrium doping amount as well as hydrothermal temperature; thereafter particle size and crystal structures of the products were studied.

2. Experimental section

Yttria stabilized zirconia nanocrystals were prepared by hydrothermal synthesis using a flow reaction system. Zirconium oxynitrate (97% $ZrO(NO_3)_2 2H_2O$; Wako Pure Chemicals Co. Ltd.), yttrium nitrate hexahydrate (99.9% $Y(NO_3)_3 6H_2O$; Wako Pure Chemicals Co. Ltd.) and potassium hydroxide (85% KOH; Wako Pure Chemicals Co. Ltd.) were used as starting materials. The Zr and Y mixed salts were dissolved into deionized water, and the total concentration of Zr and Y was adjusted to 0.1 M with the variation of yttrium molar ratio from 3% to 9%. Schematic diagram of the flow reactor system used in this study is shown in Fig. 1. Each Zr/Y mixed solution and KOH solution were fed forward to a reactor by high-pressure pump at a total flow rate of 8 g/min, and these two streams were mixed at the first mixing tee, MP1. On the other hand, deionized water was fed by another high-pressure pump at a flow rate of 22 g/min and heated to an appropriate temperature by an electric cyclic furnace through 1/8″ in Inconel tube with 30 m in length. The reactant mixture of Zr/Y mixed solution and KOH solution was mixed with the supercritical water at the second mixing tee, MP2. The rapid heating can be achieved by mixing with the supercritical water within 10 ms since the supercritical water was turbulent flow under the present flow conditions. The reaction temperatures were 300, 350, and 400 °C and pressure was set to be 30 MPa. As soon as the reactant reached the desired temperature, hydrothermal reaction took place and YSZ nanoparticles formed. The reactant was maintained in a 1/16″ in SUS tube reactor with a 1.0 mm inner diameter and a 30 cm length. The reaction time (residence time), t, was defined as follows:

$$t = V\rho/F \quad (1)$$

where V is the reactor volume (0.236 cm^3), F is flow rate (0.5 g/s) and ρ is the solution density (g/cm^3) at the constant temperature and pressure. In this study, since the precursor solution is diluted with supercritical water, density of pure water was considered to evaluate the reaction time. Densities of water under constant pressure of 30 MPa were 0.751, 0.644 and 0.357 g/cm^3 at 300, 350 and 400 °C, respectively. Reaction time was 0.35, 0.30, and 0.17 s at 300, 350 and 400 °C, respectively. After the prescribed reaction time period, hydrothermal reaction was quenched by cooling at the end of the reactor. The reactant solution was then depressurized with a back pressure regulator. The each reaction run was allowed to continue for 30 min without any blockages in the mixer. The YSZ nanoparticles dispersed solutions were filtered with 0.025 μm membrane filter to recover the solid products. The solid was washed with deionized water and pure ethanol to remove ionic impurities.

Conversion of metal ions into solid product was defined by

$$Y = (1 - C/C_0) \times 100 \quad (2)$$

where C and C_0 are molal concentrations of the metal species in the recovered and feed solutions, respectively. The conversions of Zr and Y ions were estimated from the concentrations of metal ions in the filtrate measured with an inductively coupled plasma atomic emission spectrometry (ICP-AES), using a Seiko instruments SPS7800. The recovered solid products were dried at 60 °C for 1 day. The crystal structure of the products was determined by X-ray diffraction measurement (XRD; Rigaku Co. Ltd., Model RINT 2000). Raman spectroscopy was carried out on a JASCO model NRS-3100 using a 100 mW laser with a wavelength of 532 nm. The particle size in a dispersed solution was evaluated with the dynamic light scattering technique (abbreviated as DLS) (Photal Otsuka Electronics Co, FDLS-3000). Particle size and the morphology of the obtained particles were examined by transmission electron microscopy (TEM; FEI Co., Model TECNAI-G2). BET surface area of the particles was measured by nitrogen adsorption measurement (QUANTACHROME Co., CHEMBET 3000). The calculation for the mean particle size [D] from the BET surface area is described in the equation $D = 6000/s\rho$, where s is BET surface area (m^2/g) and ρ is the density of $Zr_{0.92}Y_{0.08}O_{1.96}$ [5.9 g cm^{-3}] using crystal lattice density in PDF file 48-224. Thermogravimetric analysis was performed using a Bruker TG-DTA simultaneous thermal analyzer (model 2000SA) at a heating rate of 10 K/min to determine the water content of as-prepared powders. The chemical compositions of the solid samples were confirmed by SEM-EDS measurements (JEOL JSM-5600) for the major elements. The Y/Zr molar ratios estimated from ICP analyses from filtrate solutions were consistent with those measured by SEM-EDS within the experimental error intrinsic to the method.

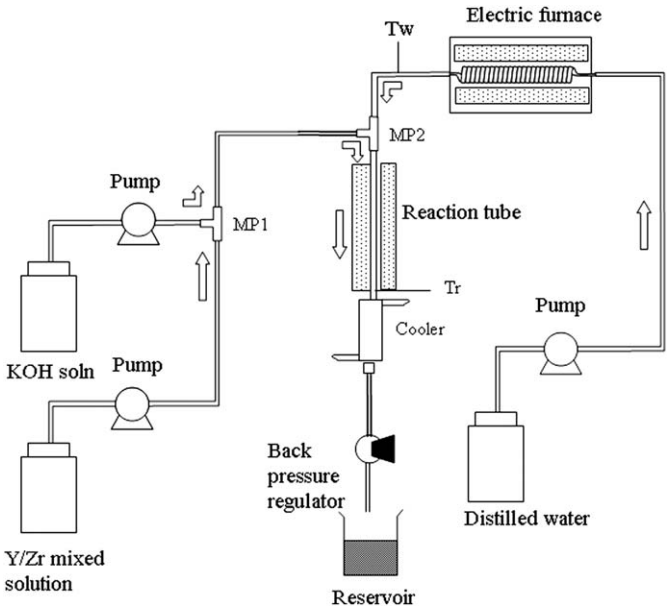

Fig. 1. Schematic diagram of the flow reactor system.

3. Results and discussion

3.1. Effect of pH on the YSZ nanoparticles formation

Fig. 2 shows conversion of zirconium and yttrium ions as a function of pH. The conversion of Zr was almost 100% irrespective of pH and reaction temperature, whereas the conversion of yttrium increased with increase in pH and reached 100% at pH 8

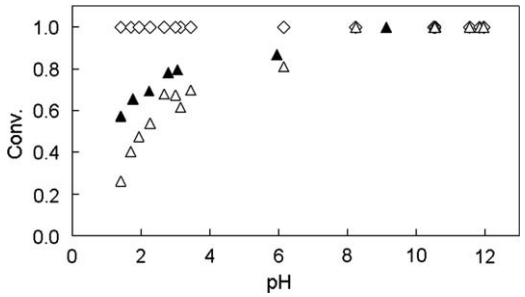

Fig.2. Conversion of Zr, Y as the function of pH. ◇, Zr (350,400 °C); ▲, Y (400 °C); △, Y (350 °C).

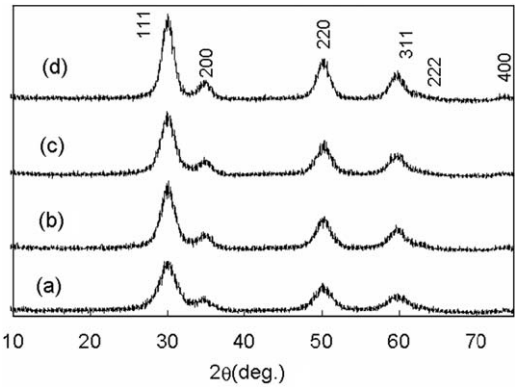

Fig.3. XRD profiles of YSZ nanoparticles synthesized at 400 °C, 30 MPa with the variation of pH. (a) pH 1.4, (b) pH 3.1, (c) pH 5.9, (d) pH 9.1. Yttria molar ratio:6 mol%.

or higher. In addition, the conversion of yttrium in the lower pH range at 400 °C was higher than that at 350 °C. Based on the relationship between the conversion and the solubility of metal oxide, conversion of zirconia is much higher among the various metal oxides [38]. Hydrolysis of Zr(IV) occurs in strongly acidic solutions and is dominated by the formation of polymeric species such as $Zr_3(OH)_4^{8+}$ or $Zr_4(OH)_8^{8+}$. The amorphous zirconium hydrous oxides are precipitated near pH 2 and are slightly soluble in base. In contrast, since yttrium ion is fairly large (0.92 A), hydrolysis in solution does not become appreciable until fairly high pH values are reached (>6). Thus, yttrium ion is stable in the low pH region. Accordingly, pH is a key factor to dope yttrium into zirconia particles stoichiometrically.

The formation mechanism of YSZ nanoparticles can be addressed as follows: At first, $Zr_4(OH)_8^{8+}$ and Y^{3+} ions are expected to hydrolyze simultaneously to (Zr,Y)-hydroxide at mixing point 1 and possibly form complexes with OH^- ions and/or H_2O molecules, such as $[Zr(OH)_5]^-$ and $Y(OH)_4^-$ which may transform into polymeric complexes. Upon mixing with supercritical water, further polymerization between the Zr and Y species is likely to occur via –OH bridging during structural rearrangement, and finally this could lead to the formation of an ordered structure by the dehydration of the surface hydroxyl of the YSZ crystallite. Accordingly, it is possible for the hydrous (Zr,Y)-oxide to crystallize into YSZ nanoparticles via heterogeneous nucleation-growth (in situ transformation mechanism) under sub- and supercritical conditions.

Fig. 3 shows XRD patterns of the product powders synthesized at 400 °C with various pH. Broad reflection peaks can be indexed by the fluorite-type cubic structure. No extra peaks were detected

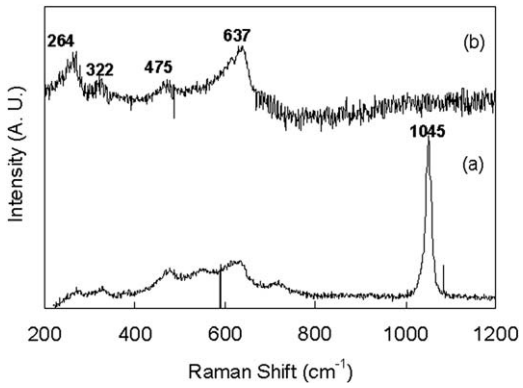

Fig. 4. Raman spectra of YSZ nanoparticles synthesized at 400 °C, 30 MPa: (a) as prepared (pH 3.1), (b) calcined at 900 °C. Yttria molar ratio: 6 mol%.

for yttria and monoclinic zirconia indicating that yttria zirconia solid solution was successfully formed, even if the reaction time was as short as 0.17 s. The peak intensity slightly increased with the solution pH indicating higher crystallinity of the sample synthesized in higher pH medium. It might be accepted that crystallinity increases with increasing pH value, since OH^- bondings alter into O^{2-} ones in high range of pH [39]. However, peak broadening was appreciable presumably due to the small crystallite size, there was little evidence for peak splitting which is specific to the tetragonal ZrO_2. In addition, lattice parameters calculated from the representative XRD profile became $a = 5.14$ and $c = 5.16$. Compared with those tetragonal ZrO_2 ($a = 5.12$, $c = 5.25$), the c/a ratio was close to unity, which is classified as tetragonal t'' form whose axial ratio equals unity. The cubic-tetragonal phase transition occurs by the oxygen displacement along the c-axis from the ideal fluorite site [40]. Thus, it is difficult to identify the tetragonal (t'' form) or fluorite-type cubic phase on the basis of the present XRD results since the XRD is not sensitive to oxygen-induced transitions.

Evidence for tetragonality in the YSZ sample can be supported by the Raman scattering technique. Fig. 4 shows Raman spectra of the samples synthesized at 400 °C (pH 3.1, 5.8 mol% Y) and the same sample after heat treated at 1000 °C. The spectra exhibited several weak peaks at 264, 322, 475 and 637 cm^{-1} which were characteristic of tetragonal zirconia corresponding to Raman-active modes of A_{1g}+3Eg+2B_{1g} symmetry [21,29]. In the case of cubic fluorite structure, only one F_{2g} mode centered at around 490 cm^{-1} is Raman active [9,16]. Thus, the YSZ samples synthesized under subcritical and supercritical water conditions are confirmed to be tetragonal phase. In the spectrum of the former sample, the strong band was observed at 1045 cm^{-1}, which is attributable to the nitrate groups [41]. The peak for nitrate groups was observed only for the samples synthesized in acidic solutions (pH$<$4). The nitrate anions are adsorbed on the zirconium oxide surfaces at lower pH as counter ions. Surface charge of the particles can affect the colloidal dispersion in the solutions. In the present synthesis experiments, recovering solution at low pH was stable as dispersed solution without precipitate whereas the particles from the solution at higher pH readily settled down. Fig. 5 shows the pH dependence on the dispersed particle sizes measured by dynamic light scattering (DLS) technique. The average DLS particle size tends to increase from 100 to 200 nm with the solution pH in 1.3–3.3. Isoelectric point of zirconia is known to be 7–8 [1]; thus, in this pH region, surface positive electrostatic charge decreases with an increase in the solution pH and particles might be aggregated as pH increases. The aggregation of the particles was supported by the TEM

observations. Transmittance electron micrographs of particles obtained by hydrothermal flow reaction system at 400 °C with the solution pH in 1.8–5.9 are shown in Fig. 6. An obvious agglomeration was confirmed and agglomerated particle size of the samples increased with increase in pH.

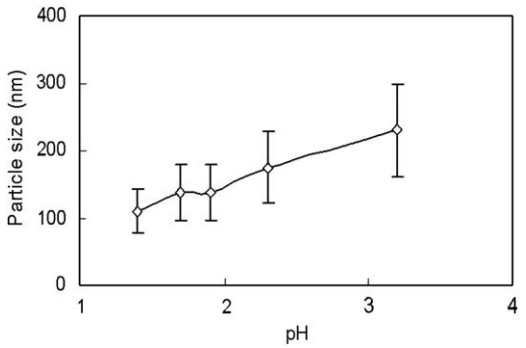

Fig. 5. Relation between solution pH and particle size from DLS result of YSZ nanoparticles dispersed solution synthesized at 400 °C, 30 MPa with the variation of pH. Yttria molar ratio: 6 mol%.

3.2. Temperature effect on the crystal phase and the particle size of YSZ

From the above paragraph, it is clear that stoichiometric doping of yttrium can be achieved under the alkaline pH conditions. Thus, YSZ nanoparticles were synthesized under subcritical and supercritical water conditions with various Y/Zr molar ratios at pH 10–11. The XRD profiles of the obtained nanoparticles by the hydrothermal reaction of Y/Zr mixed solution and KOH revealed that each diffraction peak of the particles prepared can be assigned to tetragonal phase as already mentioned, independent of Y content. Furthermore, with increase in hydrothermal temperature from 300 to 400 °C, peak intensities slightly increased and its peaks became sharp. Since XRD patterns in the absence of yttrium revealed that monoclinic phase predominated, yttrium doping is effective to stabilize the tetragonal structure.

Fig. 7 shows transmittance electron micrographs of particles obtained by hydrothermal flow reaction system at 300, 350 and 400 °C. Highly crystalline particles were obtained in spite of an obvious agglomeration. Average particle size of the samples increased with increase in hydrothermal temperature, whereas most of the particle sizes were less than 10 nm with a relatively narrow particle size distribution. Fig. 8 shows BET surface area for the powder samples as a function of hydrothermal temperature.

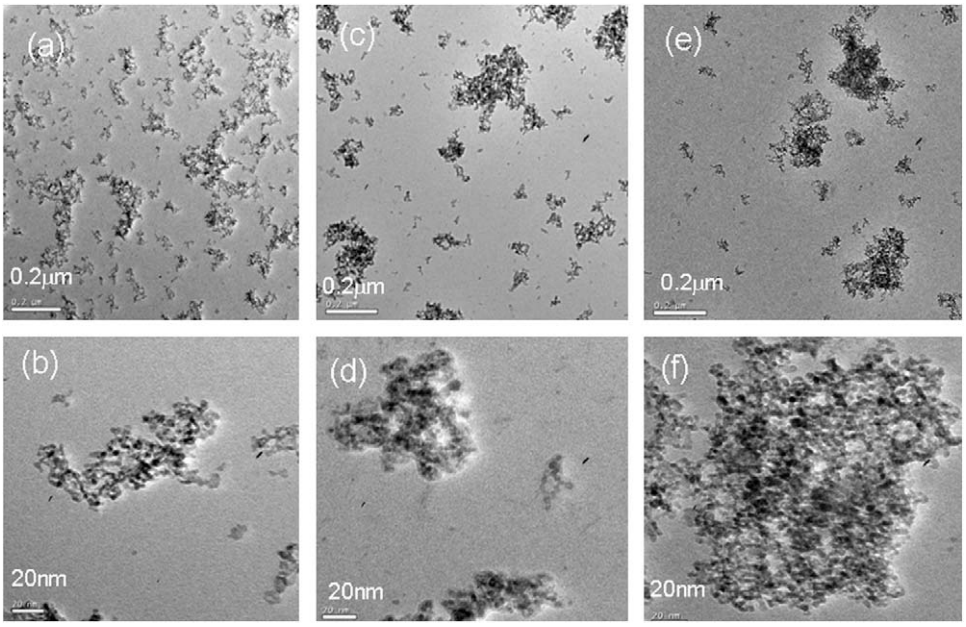

Fig. 6. TEM images of YSZ nanoparticles synthesized at 400 °C, 30 MPa with the variation of pH. (a,b) pH 1.8, (c,d) pH 2.8, (e,f) pH 5.9. Yttria molar ratio: 6 mol%.

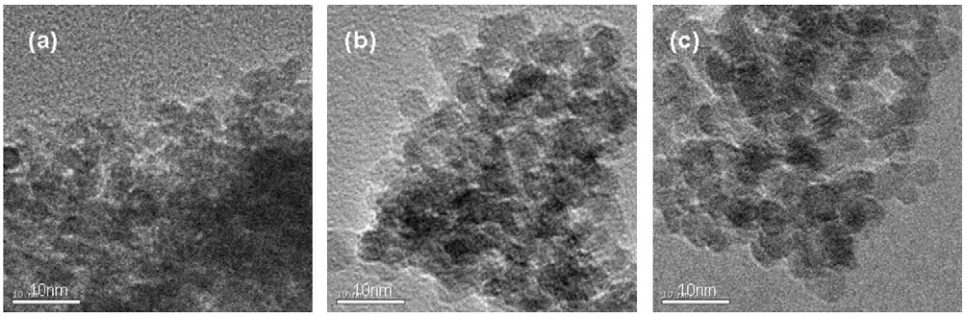

Fig. 7. TEM images of YSZ nanoparticles synthesized at (a) 300, (b) 350, (c) 400 °C, 30 MPa , pH 10–11. Yttria molar ratio: 6 mol%.

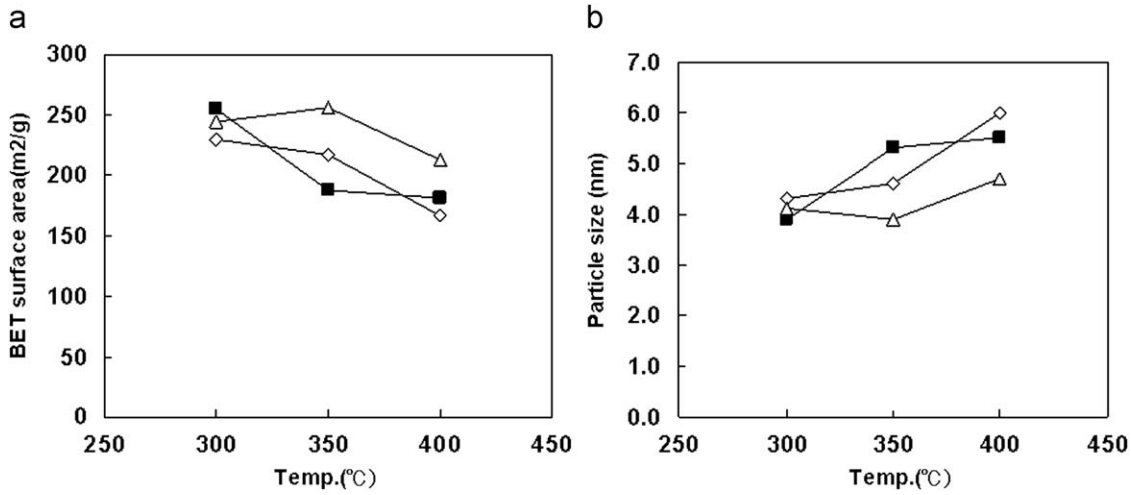

Fig. 8. Relation between hydrothermal temperature and BET surface area (a), particle size (b) of YSZ nanoparticles synthesized at pH 10–12 with the variation of Y molar ratio. ◇, 3 mol%, ■, 6mol%, △, 9 mol%.

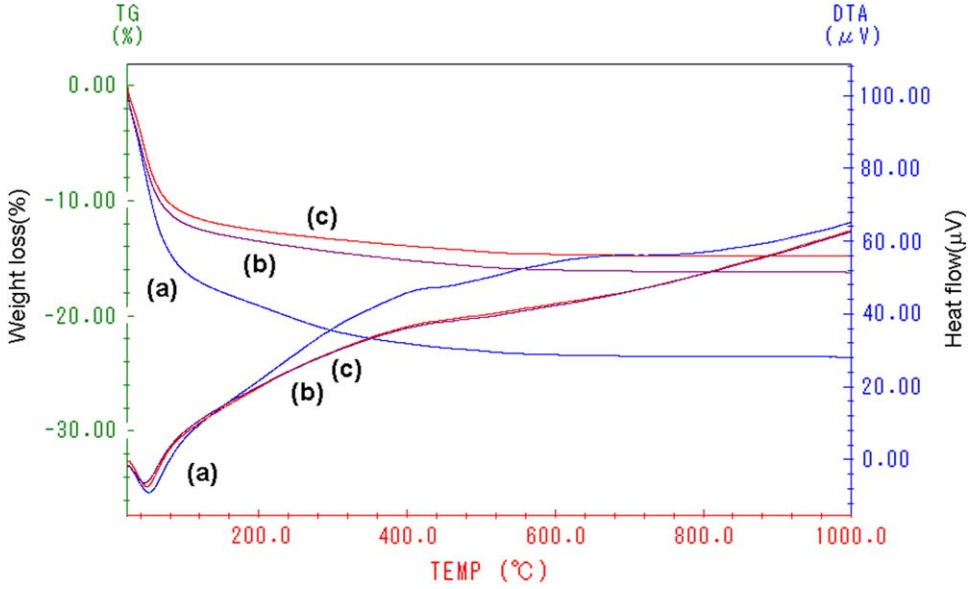

Fig. 9. TG-DTA curves for YSZ nanoparticles synthesized at pH 10–12, (a) 300, (b) 350, (c) 400 °C, 30 MPa. Y molar ratio: 6 mol%.

The BET surface area tends to decrease with increase in hydrothermal temperature irrespective of yttria molar ratio. By the calculation from BET surface area, the average particle sizes were around 4–6 nm, which are in accord with those observed in TEM images. In contrast, the crystallite sizes calculated by the Scherrer equation to the strongest PXRD peak (111) were somewhat smaller (1.4–4.2 nm). However, the trends of the crystallite sizes are the same as those of average particle sizes calculated from BET surface area where the crystallite size increased with increase in hydrothermal temperature. The particle size synthesized at higher temperature is somewhat larger irrespective of shorter reaction time presumably due to higher crystallization rate.

Thermogravimetric analysis was performed on the fresh samples. Each sample was heated in nitrogen flow from room temperature to 1000 °C, at a rate of 10 °C/min. TG-DTA curves for the YSZ samples (yttria molar ratio: 6 mol%) synthesized at 300,

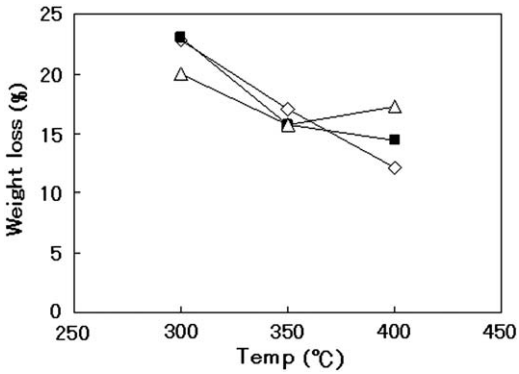

Fig. 10. Relation between hydrothermal temperature and weight loss of YSZ nanoparticles synthesized at pH10–12 with the variation of Y molar ratio. ◇, 3 mol%, ■, 6 mol%, △, 9 mol%.

350 and 400 °C are shown in Fig. 9. A decrease in the sample weight was seen at elevation temperature up to 600 °C. There was appreciable weight loss below 110 °C accompanied with an endothermic peak in DTA curve, presumably due to adsorbed water. The subsequent loss up to 600 °C was attributable to the surface hydroxyl groups. The weight losses tend to decrease with increase in reaction temperature, indicating that the surface hydroxyl groups enable the condensation to proceed under subcritical and supercritical water conditions. Weight losses amounts for the YSZ powder samples as a function of hydrothermal temperature are shown in Fig. 10. The figure shows the relation between weight losses up to 600 °C for the samples with various yttria molar ratios and the hydrothermal temperature. The weight losses tend to decrease with increase in the hydrothermal temperature irrespective of the yttria molar ratio.

4. Conclusions

Yttria stabilized zirconia nanoparticles were prepared by hydrothermal flow reaction system under 30 MPa in the temperature range 300–400 °C and pH range 1–11. The effects of pH and temperature on the Y conversion and particle size were studied. It is found that Y conversion increased with increase in solution pH and hydrothermal temperature. Stoichiometric Y/Zr solid solution can be achieved at pH 8 or higher. Primary particle sizes of YSZ estimated from BET surface area were in the range 4–6 nm irrespective of solution pH and hydrothermal temperature. However, secondary particle sizes measured by dynamic light scattering technique increased with solution pH since aggregation was appreciable as pH increased since the repulsion force weaken as pH increased. The phase stabilization of yttria doping demonstrated in this work is fundamentally important, which allows understanding of rapid synthesis of tetragonal zirconia nanoparticles for technological applications. Further investigation seems to be necessary to make clear the correlation between crystal phase transformation and displacement of oxygen into hydroxyl group.

Acknowledgments

This work was financially supported by the Budget for Minimum Energy Research of the Ministry of Economy, Trade and Industry.

References

[1] M.J. Mayo, J.R. Seidensticker, D.C. Hague, A.H. Carim, Nano Struct. Mater. 11 (2) (1999) 271–282.
[2] X. Yang, R.E. Jentoft, F.C. Jentoft, Catal. Lett. 106 (2006) 195–202.
[3] Y. Sun, S. Walspurger, B. Louis, J. Sommer, Appl. Catal. A: General 292 (2005) 200–207.
[4] M. Faticanti, N. Cioffi, S. De Rossi, N. Ditaranto, P. Porta, L. Sabbatini, T. Bleve-Zacheo, Appl. Catal. B: Environ. 60 (2005) 73–82.
[5] O.K. Tana, W. Caob, Y. Hua, W. Zhu, Solid State Ionics 172 (2004) 309–316.
[6] G. Liu, Y. Lin, Anal. Chem. 77 (2005) 5894–5901.
[7] Q. Zhu, B. Fan, Solid State Ionics 176 (2005) 889–894.
[8] S.T. Aruna, K.S. Rajam, Scripta Mater. 48 (2003) 507–512.
[9] M. Hirano, K. Hirai, J. Nanopart. Res. 5 (2003) 147–156.
[10] M. Hirano, T. Miwa, M. Inagaki, J. Solid State Chem. 158 (2001) 112–117.
[11] M.Z.-C. Hu, M.T. Harris, C.H. Byers, J. Colloid Inter. Sci. 198 (1998) 87–99.
[12] B. Ksapabutr, E. Gulari, S. Wongkasemjit, Mater. Chem. Phys. 83 (2004) 34–42.
[13] M. Eslamian, M. Ahmed, N Ashgriz, Nanotechnology 17 (2006) 1674–1685.
[14] M.C. Heine, L. Mädler, R. Jossen, S.E. Pratsinis, Combust. Flame 144 (2006) 809–820.
[15] A. C-Evulet, V. Shukla, N.G. Glumac, B. Kear, F. Cosandey, Scripta Mater. 44 (2001) 2259–2262.
[16] D.G. Lamas, G.E. Lascalea, R.E. Juárez, E. Djurado, L. Pérez, N.E. Walsöe de Reca, J. Mater. Chem. 13 (2003) 904–910.
[17] S. Shukla, S. Seal, R. Vij, S. Bandyopadhyay, J. Nanopart. Res. 4 (2002) 553–559.
[18] S.R. Dhage, S.P. Gaikwad, P. Muthukumar, V. Ravi, Mater. Lett. 58 (2004) 2704–2706.
[19] Y.-W. Zhang, Z.-G. Yan, F.-H. Liao, C.-S. Liao, C.-H. Yan, Mater. Res. Bull. 39 (2004) 1763–1777.
[20] Y. Zhang, A Li, Z. Yan, G. Xu, C. Liao, C. Yan, J. Solid State Chem. 171 (2003) 434–438.
[21] M. Kakihana, S. Kato, M. Yashima, M. Yoshimura, J. Alloys Compd. 280 (1998) 125–130.
[22] L. Combemale, G. Caboche, D. Stuerga, D. Chaumont, Mater. Res. Bull. 40 (2005) 529–536.
[23] M. Yoshimura, S. SoÅmiya, Mater. Chem. Phys. 61 (1999) 1–8.
[24] R. Piticescu, C. Montyb, D. Millers, D. Millers, Sensors Actuators B 109 (2005) 102–106.
[25] Y.V. Kolen'ko, V.D. Maximov, A.A. Burukhin, V.A. Muhanov, B.R. Churagulov, Mater. Sci. Eng. C 23 (2003) 1033–1038.
[26] R.M Piticescu, R.R. Piticescu, D Taloi, V Badilita, Nanotechnology 14 (2003) 312–317.
[27] C. Kaya, J.Y. He, X. Gu, E.G. Butler, Micropor. Mesopor. Mater. 54 (2002) 37–49.
[28] Y.-W. Zhang, X. Sun, G. Xu, S.-J. Tian, C.-S. Liao, C.-H. Yan, Phys. Chem. Chem. Phys. 5 (2003) 2129–2134.
[29] H. Wang, G. Li, Y. Xue, L. Li, J. Solid State Chem. 180 (2007) 2790–2797.
[30] Y.-W. Zhang, X. Sun, G. Xu, C.-H. Yan, Solid State Sci. 6 (2004) 523–531.
[31] P.E. Meskin, V.K. Ivanov, A.E. Barantchikov, B.R. Churagulov, Y.D. Tretyakov, Ultrasonics Sonochem. 13 (2006) 47–53.
[32] Y. Zhang, G. Xu, Z. Yan, Y. Yang, C. Liao, C. Yan, J. Mater. Chem. 12 (2002) 970–977.
[33] E. Lester, P. Blood, J. Denyer, D. Giddings, B. Azzopardi, M. Poliakoff, J. Supercrit, Fluids 37 (2006) 209–214.
[34] Y. Hakuta, T. Ohashi, H. Hayashi, K. Arai, J. Mater. Res. 19 (2004) 2230–2234.
[35] A. Cabanas, J.A. Darr, E. Lester, M. Poliakoff, Chem. Commun. (2000) 901–902.
[36] A. Cabanas, J.A. Darr, E. Lester, M. Poliakoff, J. Mater. Chem. 11 (2001) 561–568.
[37] X. Weug, J.K. Cockcroft, G. Hyett, M. Vickers, P. Boldrin, C.C. Tang, S.P. Thompson, J.E. Parker, J.C. Knowles, I. Rehman, I. Parkin, J.R.G. Evans, J.A. Darr, J. Comb. Chem. (doi:10.1021/cc900041a).
[38] K. Sue, M. Suzuki, K. Arai, T. Ohashi, H. Ura, K. Matsui, Y. Hakuta, H. Hayashi, M. Watanabe, T. Hiaki, Green Chem. 8 (2006) 634–638.
[39] T. Tsukada, S. Venigalla, A.A. Morrone, J.H. Adair, J. Am. Ceram. Soc. 82 (5) (1999) 1169–1173.
[40] M. Yashima, M. Kakihana, M. Yoshimura, Solid State Ionics 86–88 (1996) 1131–1149.
[41] P.D. Southon, J.R. Bartlett, J.L. Woolfrey, B. Ben-Nissan, Chem. Mater. 14 (2002) 4313–4319.